

Gallium(III)- and Thallium(III)-Encapsulated Polyoxopalladates: Synthesis, Structure, Multinuclear NMR, and Biological Activity Studies

Tian Ma, Xiang Ma, Zhengguo Lin,* Jiayao Zhang, Peng Yang, Tibor Csupász, Imre Tóth,* Sonja Misirlic-Dencic, Andjelka M. Isakovic, David Lembo, Manuela Donalizio, and Ulrich Kortz*

Cite This: *Inorg. Chem.* 2023, 62, 13195–13204

Read Online

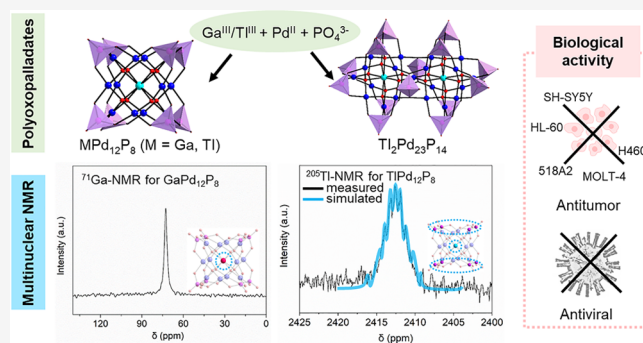
ACCESS |

Metrics & More

Article Recommendations

Supporting Information

ABSTRACT: Three gallium(III)- and thallium(III)-containing polyoxopalladates (POPs) have been synthesized and structurally characterized in the solid state and in solution, namely, the phosphate-capped 12-palladate nanocubes $[\text{XPd}_{12}\text{O}_8(\text{PO}_4)_8]^{13-}$ ($\text{X} = \text{Ga}^{\text{III}}$, $\text{GaPd}_{12}\text{P}_8$; $\text{X} = \text{Tl}^{\text{III}}$, $\text{TlPd}_{12}\text{P}_8$) and the 23-palladate double-cube $[\text{Tl}_2^{\text{III}}\text{Pd}_{23}\text{P}_{14}\text{O}_{70}(\text{OH})_2]^{20-}$ ($\text{Tl}_2\text{Pd}_{23}\text{P}_{14}$). The cuboid POPs, $\text{GaPd}_{12}\text{P}_8$ and $\text{TlPd}_{12}\text{P}_8$, are solution stable as verified by the respective ^{31}P , ^{71}Ga , and ^{205}Tl nuclear magnetic resonance (NMR) spectra. Of prime interest, the spin–spin coupling schemes allowed for an intimate study of the solution behavior of the Tl^{III} -containing POPs via a combination of ^{31}P and ^{205}Tl NMR, including the stoichiometry of the major fragments of $\text{Tl}_2\text{Pd}_{23}\text{P}_{14}$. Moreover, biological studies demonstrated the antitumor and antiviral activity of $\text{GaPd}_{12}\text{P}_8$ and $\text{TlPd}_{12}\text{P}_8$, which were validated to be as efficient as *cis*-platinum against human melanoma and acute promyelocytic leukemia cells. Furthermore, $\text{GaPd}_{12}\text{P}_8$ and $\text{TlPd}_{12}\text{P}_8$ exerted inhibitory activity against two herpes viruses, HSV-2 and HCMV, in a dose–response manner.



INTRODUCTION

Polyoxometalates (POMs) are discrete, anionic metal–oxo clusters mainly comprising edge- or corner-shared MO_6 octahedra of early *d*-block metal ions in high oxidation states (e.g., $\text{M} = \text{W}^{\text{VI}}$, Mo^{VI} , V^{V}), featuring a broad diversity of structures and compositions combined with potential in fundamental and applied science.¹ For example, in many studies, the biomedical potential of POMs was evaluated and, in some cases, promising antimicrobial properties, such as antibacterial, antiviral, and antitumor, were detected.² The POM subclass of polyoxopalladates (POPs), based on square-planar oxo-coordinated Pd^{II} addenda, was discovered in 2008 and has since been developed further systematically, leading to almost 100 polyanions of various composition, shape and size.³ Almost all POP salts are soluble and solution stable in water, allowing for biomedical, catalytic, and electrochemical studies.⁴

In 2008, the first POP was reported, $[\text{Pd}_{13}\text{As}_8\text{O}_{34}(\text{OH})_6]^{8-}$ ($\text{Pd}_{13}\text{As}_8$), which has a cuboid shape with an edge length of ca 1 nm.⁵ Following this milestone discovery, the class of POPs has been developed systematically, leading to many derivatives of the $\text{Pd}_{13}\text{As}_8$ nanocube with various central metal ion guests and different types of capping groups, as well as the discovery of other structural types, such as the 15-palladate nanostar,^{6a,b} the Sr^{2+} -centered 12-palladate open-shell structure,^{6c} and a wheel-shaped structure.^{6d} Recently, neutral and even cationic

palladium-oxo clusters (POCs) were reported.⁷ Previous work reported on the theoretically predicted followed by the successful experimental incorporation of tri- and tetravalent main group cations (e.g., Ga^{III} , In^{III} , Tl^{III} , Sn^{IV} , Pb^{IV}) inside the Pd_{12} host shell.⁸ Experimental results have documented that the addition of main group metals such as Sn^{IV} and Pb^{IV} to POPs could act as promising antileukemic agents, causing oxidative stress-mediated, caspase-dependent DNA fragmentation, accompanied with phosphatidyl serine externalization, all signifying apoptosis of leukemic cells.⁹ Moreover, the Tl^{III} -containing polyoxotungstates $[\text{Tl}_2^{\text{III}}\{\text{B-}\beta\text{-SiW}_8\text{O}_{30}(\text{OH})\}_2]^{12-}$ and $[\text{Tl}_2^{\text{III}}\text{Na}_2(\text{H}_2\text{O})_2\{\text{P}_2\text{W}_{15}\text{O}_{56}\}_2]^{16-}$ were shown to possess promising biological activity.¹⁰

Based on these findings, the complexation of Ga^{III} and Tl^{III} ions in POPs might not only be promising from a structural point of view but also lead to a class of biofunctional materials. Herein, we report on the synthesis of novel gallium- and

Received: May 10, 2023

Published: August 9, 2023



Table 1. Crystal Data and Structure Refinement for Na₁₃[Ga^{III}O₈Pd₁₂(PO₄)₈]·50H₂O (Na-GaPd₁₂P₈), Na₁₃[Tl^{III}O₈Pd₁₂(PO₄)₈]·41H₂O (Na-TlPd₁₂P₈), and Na₂₀[Tl₂^{III}Pd₂₃P₁₄O₇₀(OH)₂]·55H₂O (Na-Tl₂Pd₂₃P₁₄)

compound	Na ₁₃ [GaO ₈ Pd ₁₂ (PO ₄) ₈]·50H ₂ O (Na-GaPd ₁₂ P ₈)	Na ₁₃ [TlO ₈ Pd ₁₂ (PO ₄) ₈]·41H ₂ O (Na-TlPd ₁₂ P ₈)	Na ₂₀ [Tl ₂ Pd ₂₃ P ₁₄ O ₇₀ (OH) ₂]·55H ₂ O (Na-Tl ₂ Pd ₂₃ P ₁₄)
empirical formula	Na ₁₃ GaPd ₁₂ P ₈ O ₉₀ H ₁₀₀ (Na ₁₁ GaPd ₁₂ P ₈ O ₅₇) ^c	Na ₁₃ TlPd ₁₂ P ₈ O ₈₁ H ₈₂ (Na ₁₀ TlPd ₁₂ P ₈ O ₅₀) ^c	Na ₂₀ Tl ₂ Pd ₂₃ P ₁₄ O ₁₂₇ H ₁₁₂ (Na ₂ Tl ₂ Pd ₂₃ P ₁₄ O ₇₇) ^c
formula weight, g/mol	3433.94 (2759.17) ^c	3406.45 (2758.84) ^c	5894.66 (4567.52) ^c
crystal system	cubic	cubic	orthorhombic
space group	<i>Fm-3m</i>	<i>Fm-3m</i>	<i>Cmca</i>
<i>a</i> , Å	20.0463(15)	20.0733(9)	34.2001(12)
<i>b</i> , Å	20.0463(15)	20.0733(9)	21.0768(7)
<i>c</i> , Å	20.0463(15)	20.0733(9)	20.1416(6)
α , deg	90.00	90.00	90.00
β , deg	90.00	90.00	90.00
γ , deg	90.00	90.00	90.00
volume, Å ³	8055.7(10)	8088.3(11)	14518.6(8)
<i>Z</i>	4	4	4
<i>D</i> _{calc} , g/cm ³	2.831	2.797	2.703
absorption coefficient, mm ⁻¹	3.312	4.940	5.311
<i>F</i> (000)	6664	6504	11 136
θ range for data collection, deg	2.87–28.32	1.76–28.28	2.27–28.22
completeness to Θ _{max}	99.6	99.3	99.9
index ranges	−23 ≤ <i>h</i> ≤ 21, −25 ≤ <i>k</i> ≤ 26, −12 ≤ <i>l</i> ≤ 26	−24 ≤ <i>h</i> ≤ 23, −26 ≤ <i>k</i> ≤ 9, −15 ≤ <i>l</i> ≤ 26	−45 ≤ <i>h</i> ≤ 44, −28 ≤ <i>k</i> ≤ 28, −19 ≤ <i>l</i> ≤ 26
reflections collected	7097	7585	82 064
independent reflections	564	563	9133
<i>R</i> (int)	0.0308	0.0725	0.0646
absorption correction	semiempirical from equivalents	semiempirical from equivalents	semiempirical from equivalents
data/restraints/parameters	564/0/25	563/78/37	9133/384/274
goodness-of-fit on <i>F</i> ²	1.063	1.083	1.044
<i>R</i> ₁ , ^a <i>wR</i> ₂ ^b (<i>I</i> > 2σ(<i>I</i>))	<i>R</i> ₁ = 0.0478, <i>wR</i> ₂ = 0.1706	<i>R</i> ₁ = 0.0869, <i>wR</i> ₂ = 0.2664	<i>R</i> ₁ = 0.0807, <i>wR</i> ₂ = 0.2441
<i>R</i> ₁ , ^a <i>wR</i> ₂ ^b (all data)	<i>R</i> ₁ = 0.0596, <i>wR</i> ₂ = 0.1957	<i>R</i> ₁ = 0.1039, <i>wR</i> ₂ = 0.2977	<i>R</i> ₁ = 0.1104, <i>wR</i> ₂ = 0.2806
largest diff. peak and hole, e/Å ³	3.093 and −1.768	10.827 and −5.587	10.411 and −4.518

^a*R*₁ = $\sum ||F_o| - |F_c|| / \sum |F_o|$. ^b*wR*₂ = $\{ \sum w[(F_o)^2 - (F_c)_2] / \sum w[(F_o)^2] \}^{1/2}$. ^cValues outside brackets indicate the actual formula unit and molar mass as obtained from elemental analysis for a bulk sample.

thallium-containing POPs, and their detailed structural characterization in the solid state and in solution, as well as an investigation of their biomedical properties.

EXPERIMENTAL SECTION

Materials and Physical Measurements. All reagents were purchased from commercial sources and used without further purification. The NMR samples were prepared by re-dissolving crystals in H₂O/D₂O. The NMR spectra of Na-GaPd₁₂P₈ were recorded on a 400 MHz instrument (JEOL, Model ECX) at room temperature, using 5 mm tubes for ³¹P and ⁷¹Ga NMR with resonance frequencies 162.14 MHz (³¹P) and 122.02 MHz (⁷¹Ga), respectively. The chemical shifts were reported to the references of 85% H₃PO₄ and 0.1 M acidic aqueous Ga(NO₃)₃, respectively. Typical parameters of ³¹P NMR spectra used were TD (time domain) = 8k, SW (sweep width) = −50 to 50 ppm, D1 (relaxation delay) = 1 s, p1 (pulse length) = 5.8 μs (30°), and NS (number of scans) = 134. Typical parameters of overnight ⁷¹Ga NMR spectra used were TD = 8k, SW = −50 to 150 ppm, D1 = 0.1 s, p1 = 5.1 μs (45°), and NS = 28k.

The Tl NMR spectra of Na-TlPd₁₂P₈ and Na-Tl₂Pd₂₃P₁₄ were recorded at 8.46 Tesla with a Bruker Avance DRX 360 MHz spectrometer at the University of Debrecen, using a 5 mm QNP probe for ³¹P at 145.78 MHz and by inserting a 10 mm 500 MHz broadband (BB) probe for ²⁰⁵Tl NMR and tuning the BB-channel to the frequency of ²⁰⁵Tl (208.21 MHz); no ¹H and D₂O lock channels are available at this configuration. Overnight ²⁰⁵Tl NMR spectra (p1 = 12 μs (60°), D1 = 3 s, TD = 4k, NS = 20k, experimental time = 17 h) were measured by a home-modified 5 mm indirect BB probe tunable

to ²⁰⁵Tl (208.21 MHz) using a D₂O lock. ²⁰⁵Tl NMR chemical shifts were referenced externally to infinitely diluted TlClO₄ as 0 ppm, using 50 mM Tl^I and/or Tl^{III} perchlorate solutions (Tl^I: −4.72 ppm, Tl^{III}: 2039 ppm). ³¹P longitudinal relaxation time constants (*T*₁) were determined at room temperature by an inversion recovery experiment (π -delay- $\pi/2$ pulse sequence) in pseudo two-dimensional (2D) mode provided by a Bruker Avance DRX 360 MHz spectrometer. The results were calculated by a nonlinear parameter fitting using TopSpin 3.2 software. Typical parameters used were TD = 32k, p1 = 5.6 μs (90°), and D1 = 60 s.

Fourier transform infrared spectra (FT-IR) were recorded on KBr disks by using a Nicolet-Avatar 370 spectrometer between 400 and 4000 cm⁻¹. Thermogravimetric analysis (TGA) was carried out by using a TA Instruments SDT Q600 thermobalance with a 100 mL min⁻¹ flow of dinitrogen; the temperature was ramped from 20 to 800 °C at a rate of 5 °C min⁻¹. Elemental analyses were performed by CNRS, Service Central d'Analyse, Solaize, France.

Synthesis of Na₁₃[Ga^{III}O₈Pd₁₂(PO₄)₈]·50H₂O (Na-GaPd₁₂P₈). Pd(NO₃)₂ (0.023 g, 0.102 mmol) and Ga(NO₃)₃ (0.006 g, 0.025 mmol) were dissolved in 2 mL of 0.5 M sodium phosphate solution (pH 7.0, prepared by adding NaOH solid into NaH₂PO₄ solution) at 80 °C for 60 min while stirring. Then, the solution was left to cool to room temperature before filtration. The filtrate was allowed to crystallize in an open vial. After several weeks, dark-red block-shaped crystals were obtained. The product was collected by filtration and then air-dried. Yield: 15 mg (53% based on Pd). Elemental analysis calcd (%): Ga 2.10, Pd 38.60, P 7.49, Na 9.04; found: Ga 2.20, Pd

37.90, P 7.55, Na 9.26. IR (2% KBr pellet): 1124 (s), 956 (m), 919 (m), 676 (w), 617 (s), 550 (w) cm^{-1} .

Synthesis of $\text{Na}_3[\text{Tl}^{\text{III}}\text{O}_8\text{Pd}_{12}(\text{PO}_4)_8]\cdot 41\text{H}_2\text{O}$ (Na-TIPd₁₂P₈). $\text{Pd}(\text{NO}_3)_2$ (0.023 g, 0.102 mmol) and $\text{Tl}(\text{NO}_3)_3\cdot 3\text{H}_2\text{O}$ (0.011 g, 0.025 mmol) were dissolved in 2 mL of 0.5 M sodium phosphate solution (pH 7.0) at 80 °C for 60 min while stirring. Then, the solution was left to cool to room temperature before filtration. The filtered solution was allowed to crystallize in an open vial. After leaving the solution for several weeks, dark-red block-shaped crystals were obtained. The product was collected by filtration and then air-dried. Yield: 12 mg (41% based on Pd). Elemental analysis calcd (%): Tl 6.00, Pd 37.50, P 7.27, Na 8.77; found: Tl 6.32, Pd 36.10, P 7.11, Na 9.25. IR (2% KBr pellet): 1121 (s), 1090 (sh), 968 (sh), 951 (m), 916 (m), 618 (s), 524 (m), 478 (m), 405 (m) cm^{-1} .

Synthesis of $\text{Na}_{20}[\text{Tl}_2^{\text{III}}\text{Pd}_{23}\text{P}_{14}\text{O}_{70}(\text{OH})_2]\cdot 55\text{H}_2\text{O}$ (Na-Tl₂Pd₂₃P₁₄). $\text{Pd}(\text{NO}_3)_2$ (0.023 g, 0.102 mmol) and $\text{Tl}(\text{NO}_3)_3\cdot 3\text{H}_2\text{O}$ (0.011 g, 0.025 mmol) were dissolved in 2 mL of 0.5 M sodium phosphate solution (pH 7.0) at 80 °C for 45 min while stirring. Then, the solution pH was decreased to 4.5 using 1 M HNO_3 (aq), heated again at 80 °C for 45 min, and left to cool to room temperature before gravity filtration. The filtered solution was allowed to crystallize in an open vial. After leaving the solution for several weeks, dark-red rod-shaped crystals were obtained. The product was collected by filtration and then air-dried. Yield: 22 mg (51% based on Pd). Elemental analysis calcd (%): Tl 6.94, Pd 41.50, P 7.36, Na 7.80; found: Tl 7.39, Pd 40.90, P 8.09, Na 7.29. IR (2% KBr pellet): 1121 (s), 1078 (sh), 953(m), 914 (sh), 618 (s), 530 (sh), 446 (w) cm^{-1} .

X-Ray Crystallography. The single-crystal X-ray diffraction (XRD) data of all three compounds were collected on a Bruker Kappa X8 APEX II CCD diffractometer with graphite monochromated Mo $\text{K}\alpha$ radiation ($\lambda = 0.71073 \text{ \AA}$) at 100 K. An empirical absorption correction was applied using the SADABS program. The SHELX software package (Bruker) was used to solve and refine the structures. The structures were solved by direct methods and refined by the full-matrix least-squares method ($\sum w(|F_o|^2 - |F_c|^2)^2$) with anisotropic thermal parameters for all heavy atoms included in the model. The H atoms of the crystal waters were not located. It was not possible to locate all countercations via XRD, probably because of severe crystallographic disorder, which is a common problem in POM crystallography. Therefore, the exact number of countercations and crystal waters in the bulk compounds was determined by elemental analysis, and the resulting formula units were further used throughout the paper and in the CIF file for overall consistency. The crystal data and structure refinement for the three compounds are summarized in Table 1. Cambridge Crystallographic Data files CSD-2248051 (Na-GaPd₁₂P₈), CSD-2248265 (Na-TIPd₁₂P₈), and CSD-2248052 (Na-Tl₂Pd₂₃P₁₄) contain the supplementary crystallographic data for this paper. These data can be obtained free of charge from The Cambridge Crystallographic Data Center via www.ccdc.cam.ac.uk/.

Cell Culture and Reagents. All chemicals used in the biological experiments were from Capricorn Scientific (Ebsdorfergrund, Germany), unless stated otherwise. The human cell lines H460 (lung carcinoma), SH-SY5Y (neuroblastoma), HL-60 (acute promyelocytic leukemia), and MOLT-4 (acute lymphoblastic leukemia) were obtained from the European Collection of Animal Cell Cultures (Salisbury, U.K.). The human melanoma 518A2 cell line was a gift from Dr. Danijela Maksimovic-Ivanic (Institute for Biological Research "Sinisa Stankovic", University of Belgrade, Serbia). All cells were maintained at 37 °C in a humidified atmosphere with 5% CO_2 . The H460, HL-60, MOLT-4, and 518A2 cell lines were grown in RPMI 1640 cell culture medium supplemented with 2 mM L-glutamine and 10 mM sodium pyruvate. The SH-SY5Y cell line was maintained in Modified Eagle Medium + F12 cell culture medium (1:1) supplemented with 2 mM L-glutamine and nonessential amino acids (1%). All cell culture media were additionally supplemented with 10% fetal bovine serum and 1% antibiotic/antimycotic mixture. The cells were seeded in 96-well flat-bottom plates for the viability assessment as follows: 4×10^3 /well (518A2), 10×10^3 /well (H460), 15×10^3 /well (SH-SY5Y), 30×10^3 /well (HL-60), and 50×10^3 /well (MOLT-4). The plates were

from Sarstedt, Nümbrecht, Germany. The leukemic cells were treated for 4 h after seeding, while adherent cells (518A2, H460 and SH-SY5Y) were left to rest overnight and treated the next day. Crystals of Na-GaPd₁₂P₈ and Na-TIPd₁₂P₈ were dissolved in 60 °C PBS for 8 h with intermittent sonication for preparing stock solutions of 2.5 mM. Working solutions of Na-GaPd₁₂P₈ and Na-TIPd₁₂P₈ were made by dilution in an appropriate cell culture medium, and the cells were treated for 24 h. Each experiment contained untreated cells as a control. *cis*-Platinum (CDDP, Sigma-Aldrich, Taufkirchen, Germany), the chemotherapeutic "gold standard" of metal ion-containing drugs, was used as a positive control.

Cell Viability. The acid phosphatase (AcP) assay was used to determine the number of viable cells. The AcP assay is based on *p*-nitrophenyl phosphate hydrolysis by intracellular acid phosphatases in viable cells and subsequent production of chromogen *p*-nitrophenol. The assay was performed exactly as previously described,¹¹ and absorbances, directly proportional to the number of viable cells, were measured in an automated microplate reader (Sunrise; Tecan, Dorset, U.K.) at 405 nm. The viability of the cells was calculated as percent absorbance relative to an untreated control. Each experiment was done in three or six technical replicates two or three times independently. The concentrations of the investigated compounds that reduced the cell viability by 50%, the so-called IC₅₀ values, were calculated using GraphPad Prism software (GraphPad Prism Software Inc., San Diego, CA).

Antiviral Studies. African green monkey kidney cells (Vero) (ATCC CCL-81) were cultured in Eagle's minimal essential medium (MEM) (Sigma-Aldrich) supplemented with heat-inactivated 10% fetal bovine serum (FBS) (Sigma-Aldrich) and 1% antibiotic solution (penicillin–streptomycin, Sigma-Aldrich). Human foreskin fibroblasts (HFF-1) (ATCC SCRC-1041) at low-passage-number (<30) were grown as monolayers in Dulbecco's modified Eagle's medium (DMEM) (Sigma-Aldrich) supplemented with 15% heat-inactivated FBS (Sigma-Aldrich) and 1% antibiotic solution (penicillin–streptomycin, Sigma-Aldrich). The neurovirulent strain MS (ATCC VR-540) of Herpes Simplex Virus type 2 (HSV-2) was propagated in Vero cells at 37 °C, and the viral titer was determined by the standard plaque method and expressed as plaque-forming unit (PFU)/mL, as reported by Toujani et al.¹² A bacterial artificial chromosome–derived human cytomegalovirus (HCMV) strain Towne, incorporating the green fluorescent protein (GFP) sequence, was propagated on HFF-1.¹³ HCMV titer was determined on HFF-1 cells by fluorescence focus assay and expressed as focus-forming units (FFU)/mL. Virus stocks were maintained frozen at –80 °C. The antiviral activity of GaPd₁₂P₈, TIPd₁₂P₈ and $[\text{InO}_8\text{Pd}_{12}(\text{PO}_4)_8]^{13-}$ (InPd₁₂P₈)^{8b} was determined by plaque reduction assay for HSV-2 and by focus reduction assays for HCMV on Vero cells and HFF-1 cells, respectively. The cells were treated with increasing concentrations of POPs before, during, or after the viral infection in order to use a complete protection assay. Briefly, after a 2-h incubation of the cells with POPs, a mixture of the same concentrations of POPs and virus was added to the cells. The multiplicity of infection (MOI) was of 0.002 plaque-forming units (PFU)/cell for HSV-2 and of 0.005 focus-forming units (FFUs)/cell for HCMV. The cells were incubated at 37 °C for 2 h, then washed and overlaid with a medium containing 1.2% methylcellulose 2% FBS and serial increasing dilutions of the POPs. For HSV-2 antiviral assays, after 24 h of incubation at 37 °C, the cells were fixed and stained with 20% ethanol and 0.1% crystal violet solution, and the viral plaques were counted. For HCMV antiviral assays, after 5-day incubation at 37 °C, HCMV-infected cells were visualized as green fibroblasts by fluorescence microscopy and counted. Results were reported as percentages of plaques (for HSV-2) or fluorescent foci (for HCMV) in comparison to controls. The inhibitory concentrations of POPs that reduced viral infectivity by 50% (half-maximal effective concentration, EC₅₀) and 95% confidence intervals were calculated by GraphPad Prism software to fit a variable slope-sigmoidal dose–response curve. All experiments were conducted in triplicate. In parallel, cell viability was assessed using the [3-(4,5-dimethylthiazol-2-yl)-5-(3-carboxymethoxyphenyl)-2-(4-sulphophenyl)-2H-tetrazolium] assay, as described by Donalizio et al.¹⁴

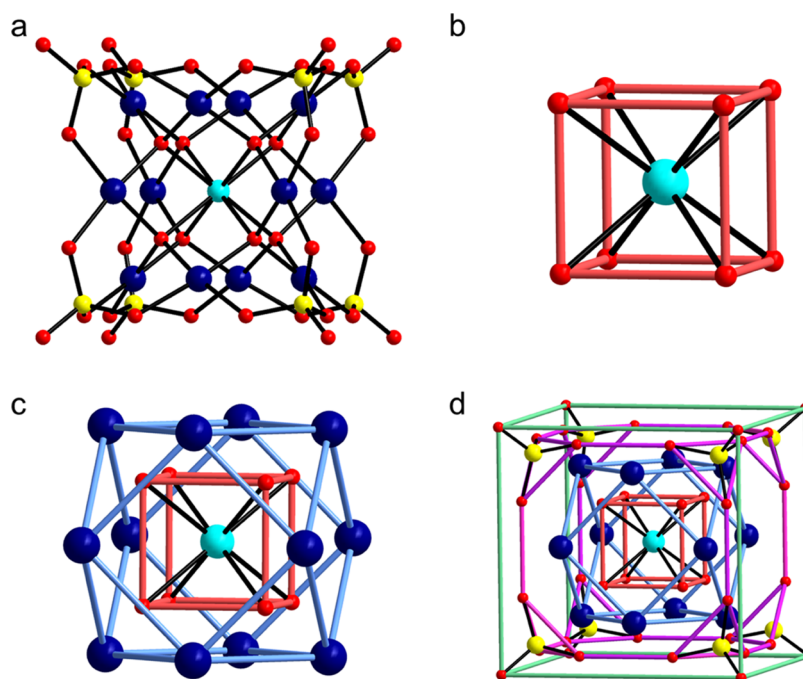


Figure 1. (a) Ball-and-stick representation of $\text{XPd}_{12}\text{P}_8$ ($X = \text{Ga}^{\text{III}}, \text{Tl}^{\text{III}}$). Color code: Ga and Tl, turquoise; Pd, blue; P, yellow; O, red. (b–d) Representation of the onion-like multishell structure of $\text{XPd}_{12}\text{P}_8$.

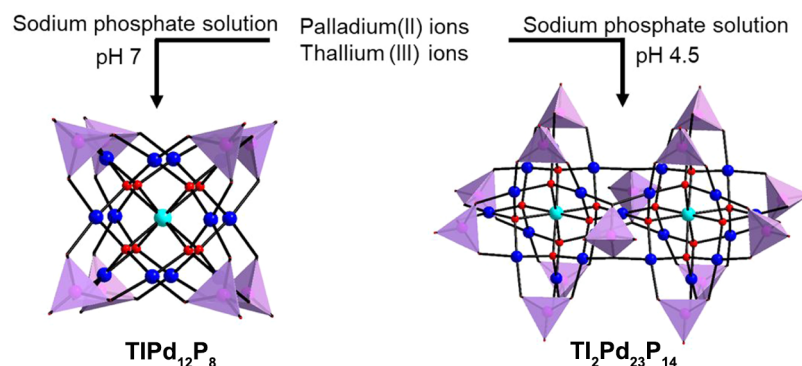


Figure 2. Synthetic scheme of polyanions $\text{TlPd}_{12}\text{P}_8$ and $\text{Tl}_2\text{Pd}_{23}\text{P}_{14}$. Color code: Tl, turquoise; Pd, blue; O, red balls; $\{\text{PO}_4\}$ tetrahedra, purple.

Briefly, confluent cells in 96-multiwell plates were cultured as for the antiviral assays. Vero cells and HFF-1 cells were incubated with serial dilutions of the POPs for 24 and 120 h, respectively. Cells viability was evaluated using the CellTiter 96 Proliferation Assay Kit (Promega), according to the manufacturer's instructions, and absorbances were measured using a Multiskan FC Microplate Photometer (Thermo Scientific). The effect of POPs on cell viability was expressed as a percentage of absorbance values of treated cells compared with those of cells incubated with culture medium alone. The 50% cytotoxic concentrations (CC_{50}) and 95% confidence intervals were determined with GraphPad Prism software by fitting a variable slope-sigmoidal dose–response curve.

RESULTS AND DISCUSSION

Synthesis and Structural Characterization. The main group metal-centered polyoxopalladates (POPs) $[\text{XO}_8\text{Pd}_{12}(\text{PO}_4)_8]^{13-}$ ($X = \text{Ga}^{\text{III}}$ ($\text{GaPd}_{12}\text{P}_8$), Tl^{III} ($\text{TlPd}_{12}\text{P}_8$)) were synthesized by the reaction of $\text{Ga}(\text{NO}_3)_3$ or $\text{Tl}(\text{NO}_3)_3 \cdot 3\text{H}_2\text{O}$ with $\text{Pd}(\text{NO}_3)_2$ in a 0.5 M sodium phosphate solution at pH 7.0 and isolated as hydrated sodium salts, $\text{Na}_{13}[\text{Ga}^{\text{III}}\text{O}_8\text{Pd}_{12}(\text{PO}_4)_8] \cdot 50\text{H}_2\text{O}$ ($\text{Na-GaPd}_{12}\text{P}_8$) and $\text{Na}_{13}[\text{Tl}^{\text{III}}\text{O}_8\text{Pd}_{12}(\text{PO}_4)_8] \cdot 41\text{H}_2\text{O}$ ($\text{Na-TlPd}_{12}\text{P}_8$), respectively.

Single-crystal X-ray diffraction revealed that the polyanions $\text{GaPd}_{12}\text{P}_8$ and $\text{TlPd}_{12}\text{P}_8$ are isostructural and they can be regarded as two new members of the POP nanocube family $\{\text{XPd}_{12}\text{L}_8\}$ ($X =$ central metal ion guest, $L =$ capping group), see Figure 1a. The guest metal ions Ga^{III} and Tl^{III} in $\text{XPd}_{12}\text{P}_8$ are coordinated by eight $\mu_4\text{-O}$ atoms to form an ideal cubic $\{\text{XO}_8\}$ coordination sphere with bond lengths $\text{Ga-O} = 2.191 \text{ \AA}$ and $\text{Tl-O} = 2.314 \text{ \AA}$, respectively (Figure 1b). This core assembly is further surrounded by 12 square-planar coordinated palladium(II) ions and capped by eight PO_4^{3-} groups to obtain a closed cuboid-shaped shell (Figure 1c,d). To date, only a handful of main group metal-centered cuboid POPs have been synthesized with phenylarsonate as the capping group ($M = \text{Ga}^{\text{III}}$ and In^{III} ; ^{8a} or Tl^{III} ¹⁵) or phosphate as the capping group (In^{III} , ^{8b} Sn^{IV} and Pb^{IV}). The crystal structures of $\text{Na-GaPd}_{12}\text{P}_8$ and $\text{Na-TlPd}_{12}\text{P}_8$ are isomorphous, see Table 1. Interestingly, a unique sodium-oxo-aqua cluster $\{\text{Na}_4\text{O}_4(\text{H}_2\text{O})_{12}\}$ was observed in the solid-state structure of $\text{Na-GaPd}_{12}\text{P}_8$ (Figure S1a). Each sodium ion is hexacoordinated in a distorted octahedral geometry by three $\mu_4\text{-oxo}$ ions (terminal oxygens of phosphate capping groups) and

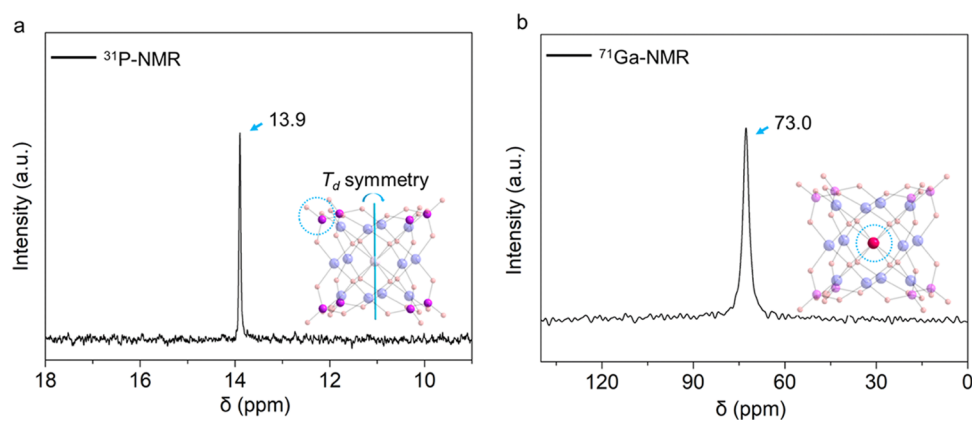


Figure 3. (a) 162.14 MHz ^{31}P NMR spectrum of $\text{Na-GaPd}_{12}\text{P}_8$ in $\text{D}_2\text{O}/\text{H}_2\text{O}$: 15 $\text{mg mL}^{-1} \approx 35$ mM for PO_4^{3-} , $\delta = 13.9$ ppm. (b) 122.02 MHz ^{71}Ga NMR spectrum of $\text{Na-GaPd}_{12}\text{P}_8$ in $\text{D}_2\text{O}/\text{H}_2\text{O}$: ~ 4.4 mM for Ga(III), $\delta = 73.0$ ppm. Inset: the structure figure of $\text{GaPd}_{12}\text{P}_8$. Color code: P, purple; Ga, red.

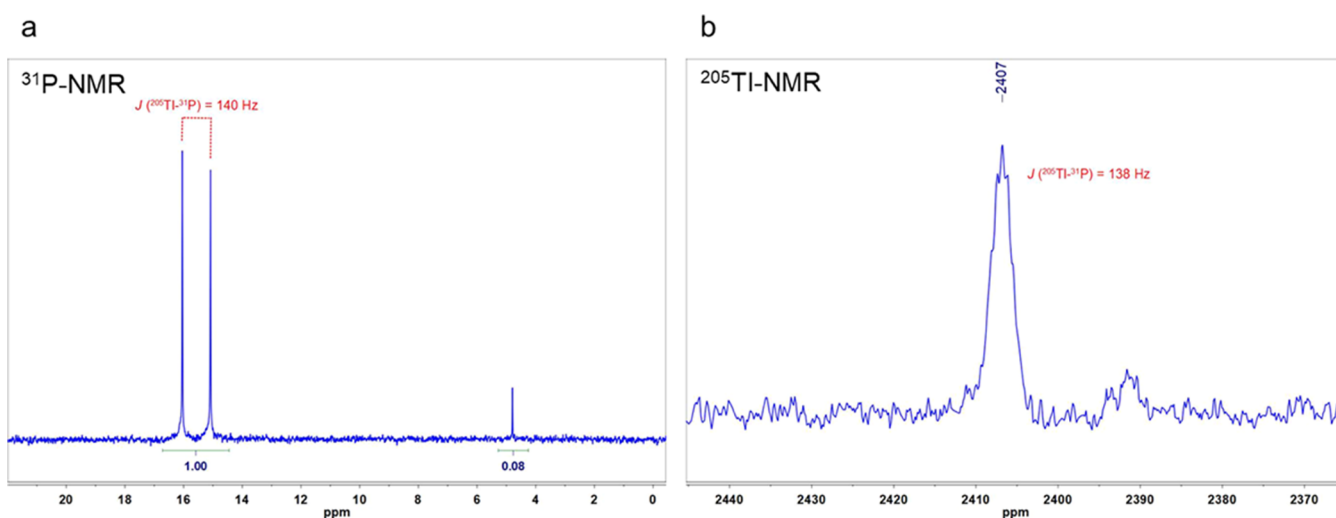


Figure 4. (a) ^{205}Tl -coupled doublet ^{31}P NMR signal (145.78 MHz) of $\text{Na-TlPd}_{12}\text{P}_8$ in water (10% D_2O): 18.5 $\text{mg mL}^{-1} \approx 43$ mM for PO_4^{3-} , $\delta = 15.6$ ppm, $^4J(^{205}\text{Tl}-^{31}\text{P}) = 140$ Hz. The small signal can be attributed to free phosphate as an impurity; estimated pH = 11. (b) ^{31}P -coupled nonet ^{205}Tl NMR signal (207.74 MHz) of the same sample: 5.3 mM for Tl(III); $\delta = 2407$ ppm, $^4J(^{205}\text{Tl}-^{31}\text{P}) = 138 \pm 10$ Hz. Minor impurities might be detected at around 2390 ppm.

three water molecules, which are interlinked with four $\text{GaPd}_{12}\text{P}_8$ polyanions (Figure S1b). Accordingly, one $\text{GaPd}_{12}\text{P}_8$ ion is connected to eight tetra-sodium clusters $\{\text{Na}_4\text{O}_4(\text{H}_2\text{O})_{12}\}$, resulting in a 3D framework (Figure S1c,d).

The double-cube $\text{Na-Tl}_2\text{Pd}_{23}\text{P}_{14}$ can only be synthesized through the reaction of $\text{Tl}(\text{NO}_3)_3 \cdot 3\text{H}_2\text{O}$ with $\text{Pd}(\text{NO}_3)_2$ in a 0.5 M sodium phosphate solution at pH 4.5, i.e., the pH is lower than that of $\text{Na-TlPd}_{12}\text{P}_8$. The synthetic scheme showcases that the pH value plays critical effects in the Tl-POP system, indicating that a lower pH is beneficial to the self-assembly of larger POPs (Figure 2). The double-cube structure of $\text{Tl}_2\text{Pd}_{23}\text{P}_{14}$ can be described as two mono-lacunary $\{\text{TlPd}_{11}\text{P}_7\text{O}_{36}\}$ units linked by an extra central Pd ion. In contrast, the reported $\text{Na}_{21}[\text{In}_2\text{Pd}_{23}\text{O}_{17}(\text{OH})(\text{PO}_4)_{12}(\text{PO}_3(\text{OH}))] \cdot 58\text{H}_2\text{O}$ ($\text{In}_2\text{Pd}_{23}\text{P}_{13}$) contains one phosphate group less (only 13 rather than 14).^{8b} Therefore, $\text{Tl}_2\text{Pd}_{23}\text{P}_{14}$ possesses higher symmetry than $\text{In}_2\text{Pd}_{23}\text{P}_{13}$. We were unable to prepare the hypothetical Ga-centered double cube, even when modifying the reaction pH to more acidic values. A possible reason could be the shorter bond lengths of Ga–O (2.191 Å) as compared to In–O (2.254 Å) and Tl–O

(2.314 Å), respectively. A decrease of the M–O bond lengths in the $\text{MPd}_{12}\text{P}_8$ family (from Tl–O via In–O to Ga–O) results in a more distorted square-planar coordination geometry around the Pd^{II} atoms, which is unfavorable for the formation of the double-cuboid structure. FT-IR spectra were recorded for all three compounds (Figure S2). The bands from 900 to 1200 cm^{-1} correspond to P–O stretching modes of the phosphate heterogroups. The other peaks below 900 cm^{-1} are attributed to Pd–O as well as to Ga/Tl–O vibrations for all three samples. Meanwhile, thermogravimetric analysis (TGA) of the crystalline compounds has been performed to investigate their thermal behavior (see Figure S3) and two weight loss steps were observed for all of them.

Multinuclear NMR Spectroscopy. To explore the solution behavior (e.g., solubility and stability) of the three POPs, we performed multinuclear NMR studies on the respective salts of POPs after re-dissolving them in $\text{H}_2\text{O}/\text{D}_2\text{O}$ at room temperature. Since $\text{GaPd}_{12}\text{P}_8$ possesses 8 chemically equivalent phosphorus atoms in the polyanion structure with a tetrahedral symmetry, the ^{31}P NMR spectrum of $\text{Na-GaPd}_{12}\text{P}_8$ exhibits a singlet at 13.9 ppm, which is in full

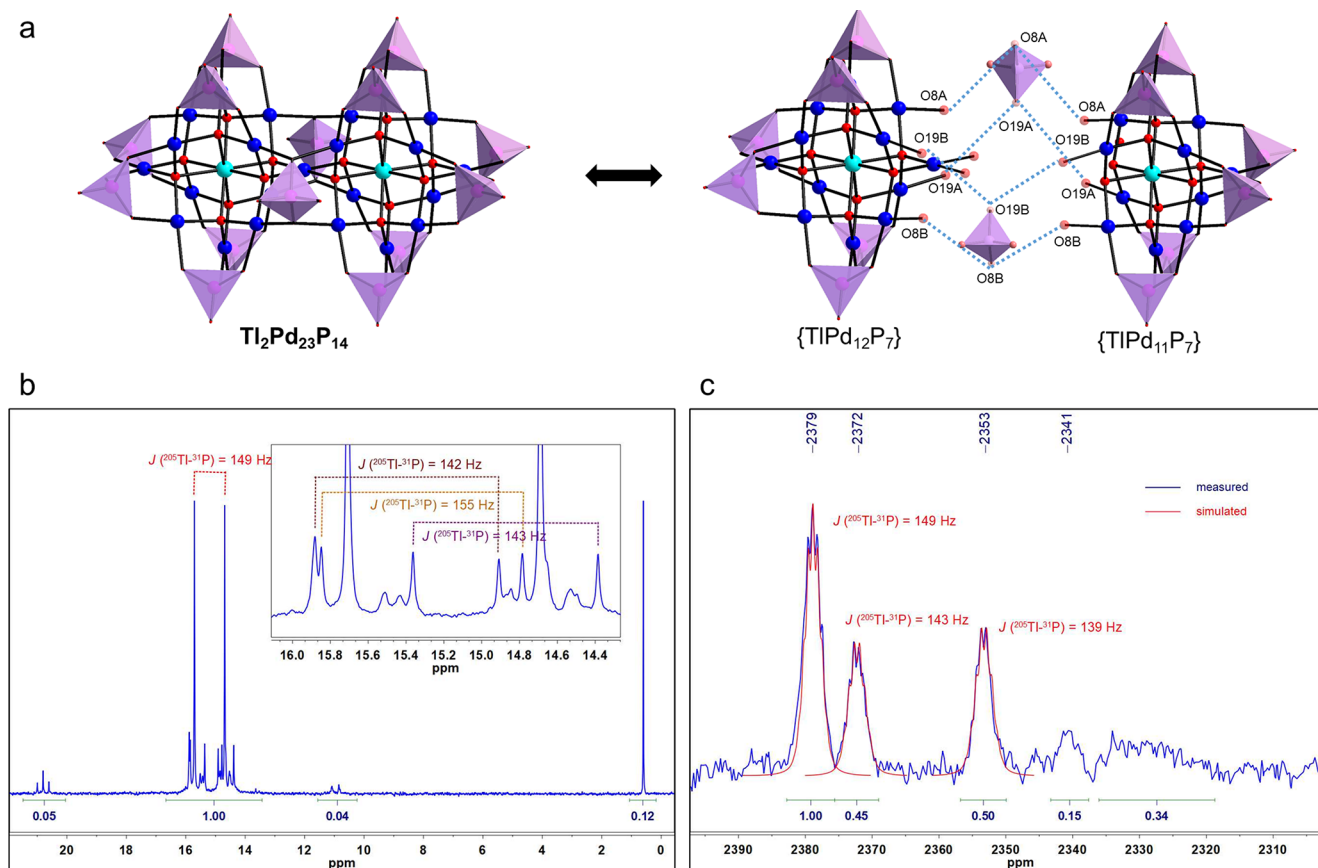


Figure 5. (a) Proposed major route of $\text{Ti}_2\text{Pd}_{23}\text{P}_{14}$ decomposition in solution. (b) ^{205}Tl -coupled ^{31}P NMR spectrum (145.78 MHz) of the disintegrated $\text{Ti}_2\text{Pd}_{23}\text{P}_{14}$ in water (10% D_2O): 22.5 mg mL^{-1} , ~ 40 mM for PO_4^{3-} . The most intense doublet at $\delta = 15.4$ ppm; $^4J(^{205}\text{Tl}-^{31}\text{P}) = 149$ Hz is attributed to the $\text{TlPd}_{12}\text{P}_8$ fragment, while doublets shown in the inset with $^4J(^{205}\text{Tl}-^{31}\text{P}) = 155$, 143, and 142 Hz are the signals of the phosphate groups in the fragments $\{\text{TlPd}_{11}\text{P}_7\}$ and $\{\text{TlPd}_{12}\text{P}_7\}$, respectively, see (a). The free phosphate is detected at $\delta = 0.6$ ppm, the estimated pH = 2. The small signals at 21 and 11 ppm can be attributed to minor impurities. (c) ^{31}P -coupled multiplets ^{205}Tl NMR signals (207.74 MHz) of the same sample: 7.6 mM for Tl^{III} ; the nonet of the $\text{TlPd}_{12}\text{P}_8$ fragment at $\delta = 2379$ ppm, $^4J(^{205}\text{Tl}-^{31}\text{P}) = 138 \pm 10$ Hz; two octets, at $\delta = 2372$ ppm, $^4J(^{205}\text{Tl}-^{31}\text{P}) = 143 \pm 10$ Hz and $\delta = 2353$ ppm, $^4J(^{205}\text{Tl}-^{31}\text{P}) = 139 \pm 10$ Hz, are assigned tentatively to the fragments $\{\text{TlPd}_{12}\text{P}_7\}$ and $\{\text{TlPd}_{11}\text{P}_7\}$, respectively. Minor impurities might be detected at around 2320–2345 ppm. The red traces (left to right) are the simulated nonet (AX_8) and two octets (AX_7), respectively.

agreement with the crystal structure (Figure 3a). Due to the highly symmetrical cubic coordination geometry of the Ga^{III} center in $\text{GaPd}_{12}\text{P}_8$, the expected narrow signal in ^{71}Ga NMR has been recorded at 73.0 ppm (Figure 3b). As one can see from Figure 3, neither the ^{31}P nor the ^{71}Ga NMR spectrum of $\text{Na-GaPd}_{12}\text{P}_8$ shows spin–spin coupling (in contrast to the analogous $\text{Na-TlPd}_{12}\text{P}_8$, see Figure 4). The lack of splitting might be attributed to the quite fast quadrupole relaxation of the central $^{71}\text{Ga}/^{69}\text{Ga}$ ($I = 3/2$) nucleus.

As expected, the ^{31}P NMR spectrum of $\text{Na-TlPd}_{12}\text{P}_8$ shows one doublet (Figure 4a) due to the spin–spin coupling ($^4J(^{31}\text{P}-^{205}\text{Tl}) = 140$ Hz) between ^{31}P ($I = 1/2$) and $^{205}/^{203}\text{Tl}$ ($I = 1/2$) nuclei. The doublet at $\delta = 15.6$ ppm can be attributed to 8 chemically equivalent phosphorus atoms coupled to one central Tl atom ($I = 1/2$ for both ^{203}Tl , 29.5% and ^{205}Tl , 70.5%). It is important to note that two different isotopologs, containing ^{205}Tl and ^{203}Tl nuclei, give separated doublets, the latter one has $^4J(^{31}\text{P}-^{205}\text{Tl}) = 138.6$ Hz, 1% smaller compared to $^4J(^{31}\text{P}-^{203}\text{Tl}) = 140$ Hz, see Figure S4. In accordance, the ^{205}Tl NMR spectrum (Figure 4b) displays the expected one signal at 2407 ppm with $^4J(^{31}\text{P}-^{205}\text{Tl}) = 138 \pm 5$ Hz, which is in reasonable agreement with the one observed in ^{31}P NMR (the larger uncertainty, about ± 5 to

Hz, of the ^{205}Tl NMR is due to the substantially larger line width (≥ 50 Hz) at the actual field strength compared to the ~ 1 Hz of ^{31}P NMR signal). These findings indicate that the cubic $\text{TlPd}_{12}\text{P}_8$ keeps the structure determined by single-crystal XRD.

Unlike the phosphate-capped nanocubic POPs with different central metal ions,^{8b,9} the multinuclear NMR results shown in Figure 5 suggest that the double-cuboid $\text{Ti}_2\text{Pd}_{23}\text{P}_{14}$ is not stable in aqueous solution. $\text{Ti}_2\text{Pd}_{23}\text{P}_{14}$ disintegrates immediately to several fragments upon re-dissolution, although the species found in solution remain constant without further decomposition for at least several weeks, according to repeated ^{31}P NMR measurements. The assignment of the complicated ^{31}P NMR spectrum is not straightforward for all signals, although the three main fragments detected by ^{205}Tl NMR can be attributed to the $^{203}/^{205}\text{Tl}$ -coupled ^{31}P NMR doublets. First of all, the most intense doublet at $\delta = 15.2$ ppm; $^4J(^{205}\text{Tl}-^{31}\text{P}) = 149$ Hz, belongs to the $\text{TlPd}_{12}\text{P}_8$ fragment. The small difference in chemical shift and $^4J(^{205}\text{Tl}-^{31}\text{P})$ compared to the values shown in Figure 4 might be explained with the acidic pH of this sample. Based on the chemical shift of free phosphate at $\delta = 0.6$ ppm, the estimated pH ~ 2 , i.e., the decomposed solution is quite acidic. The detailed examination

of the decomposition reactions is not in the scope of this work, but we suppose that some part of Tl^{III} might form mixed hydroxo species, and the released protons push the pH from neutral to acidic. The proposed major route of decomposition is shown in Figure 5a: $\text{Tl}_2\text{Pd}_{23}\text{P}_{14}$ breaks up into $\{\text{TlPd}_{11}\text{P}_7\}$ and $\{\text{TlPd}_{12}\text{P}_7\}$ fragments. It is likely that in solution the two central, bridging phosphate groups of $\text{Tl}_2\text{Pd}_{23}\text{P}_{14}$ break away from the “dimer”, mainly because the bidentate phosphate groups (coordinated atoms: O8 and O19) are not bound as strongly as the tridentate ones, resulting in the formation of two fragments, $\{\text{TlPd}_{12}\text{P}_7\}$ and $\{\text{TlPd}_{11}\text{P}_7\}$. The formation of $\text{TlPd}_{12}\text{P}_8$ from reaction of a $\{\text{TlPd}_{12}\text{P}_7\}$ fragment with a free PO_4^{3-} ion in solution is evident. Two of the three doublets with medium intensities at around 14–16 ppm and shown in the inset with $^4J(^{205}\text{Tl}-^{31}\text{P}) = 142, 143, \text{ and } 155$ might be the signals of the 4 equivalent “equatorial” phosphate groups in the fragments, $\{\text{TlPd}_{11}\text{P}_7\}$ and $\{\text{TlPd}_{12}\text{P}_7\}$, respectively, see Figure 5b, and can tentatively be attributed to the 2 equivalent “axial” phosphates, supposing coincidence of the peaks both having half-intensities. The pairing of the 6 signals with likely equal intensities to doublets is based on T_1 measurements. Signals belonging to the same doublet have equal longitudinal relaxation time constants in the range of 3.8–4.7 s and are summarized in Table S1. Two signals, the triplet at 20.8 ppm and two peaks at 11 ppm, are unknown impurities, while the smallest peaks in the doublet region (14–16 ppm) are likely the signals of the seventh phosphate groups in the $\{\text{TlPd}_{12}\text{P}_7\}$ and $\{\text{TlPd}_{11}\text{P}_7\}$ species.

Turning to the ^{31}P -coupled ^{205}Tl NMR spectrum, see Figure 5c, the nonet signal at 2379 ppm is the signal of the $\text{TlPd}_{12}\text{P}_8$ species, while $\{\text{TlPd}_{12}\text{P}_7\}$ and $\{\text{TlPd}_{11}\text{P}_7\}$ may have octet signals at 2372 and 2353 ppm, respectively. The values of $^4J(^{205}\text{Tl}-^{31}\text{P}) = 149, 143, \text{ and } 139$ Hz are in suitable agreement with the (more accurate) values measured by ^{31}P NMR. At first glance, the intensities of the multiplet peaks follow the Pascal triangle. It is obvious that $\text{TlPd}_{12}\text{P}_8$ having 8 equivalent phosphate groups forms an AX_8 spin system, but the proposed structures of the $\{\text{TlPd}_{12}\text{P}_7\}$ and $\{\text{TlPd}_{11}\text{P}_7\}$ fragments, see Figure 5a, fit to an $\text{AX}_4\text{Y}_2\text{Z}$ spin system. The clear separation of the different ^{31}P NMR signals and their narrow shape rule out any kind of internal rearrangement. Actually, the resolution of ^{205}Tl NMR is not high enough at 8.4 T to show the fine structure of the spin–spin coupling due to the chemical shift anisotropy, resulting in quite broad (50–60 Hz) signals, especially in the case of very similar coupling constants that we observed. Model calculations using the MestraNova software indicate that the shape of the overall multiplets AX_8 and $\text{AX}_4\text{Y}_2\text{Z}$ is practically identical for half-widths above 20 Hz (Figure S5). This means that the directly measured $^4J(^{205}\text{Tl}-^{31}\text{P})$ values of $\{\text{TlPd}_{12}\text{P}_7\}$ and $\{\text{TlPd}_{11}\text{P}_7\}$ from ^{205}Tl NMR are some kind of averages of the (slightly) different, “real” values, properly measurable by ^{31}P NMR.

Antitumor Activity. Considering that both $\text{Na-GaPd}_{12}\text{P}_8$ and $\text{Na-TlPd}_{12}\text{P}_8$ are solution stable in water at pH 7, it is interesting to assess their antitumor potential. Both $\text{GaPd}_{12}\text{P}_8$ and $\text{TlPd}_{12}\text{P}_8$ were fairly toxic against human melanoma (518A2), lung cancer (H460), and acute promyelocytic leukemia (HL-60), without significant differences between the two of them. Rather, low toxicity was observed for both $\text{GaPd}_{12}\text{P}_8$ and $\text{TlPd}_{12}\text{P}_8$ against human neuroblastoma (SH-SY5Y) and acute lymphoblastic leukemia (MOLT-4). However, $\text{GaPd}_{12}\text{P}_8$ showed significantly higher cytotoxic potential against MOLT-4 cells compared to $\text{TlPd}_{12}\text{P}_8$,

suggesting the specificity of $\text{GaPd}_{12}\text{P}_8$ toward acute lymphoblastic leukemia. Importantly, both $\text{GaPd}_{12}\text{P}_8$ and $\text{TlPd}_{12}\text{P}_8$ were as efficient as *cis*-platinum, the gold standard of chemotherapy, against human melanoma and acute promyelocytic leukemia cells, with IC_{50} values on human melanoma cells of the same order of magnitude as for *cis*-platinum, suggesting antimelanoma, in particular, and antileukemic potential that should be further explored. All results are summarized in Table 2.

Table 2. Antitumor Activity (IC_{50} ; 24 h) of $\text{GaPd}_{12}\text{P}_8$ and $\text{TlPd}_{12}\text{P}_8$ Determined by Acid Phosphatase Assay^a

human tumor cell lines	IC_{50} (μM)		
	$\text{GaPd}_{12}\text{P}_8$	$\text{TlPd}_{12}\text{P}_8$	CDDP
518A2	36.7 ± 1.5	25.0 ± 5.6	31.2 ± 0.9
H460	39.1 ± 4.9	39.7 ± 3.2	10.4 ± 1.3^{11a}
SH-SY5Y	87.0 ± 7.3	95.6 ± 13.8	$30.3 \pm 8.2^{\#}$
HL-60	32.5 ± 2.8	31.7 ± 8.1	17.4 ± 3.3^9
MOLT-4	69.0 ± 14.2	$112.71 \pm 29.5^*$	17.1 ± 1.6^{11b}

^aThe values presented are means \pm S.D from two or three independent experiments done in triplicate or sextuplicate; CDDP: *cis*-platinum; * $p < 0.05$ vs $\text{GaPd}_{12}\text{P}_8$; [#] $p < 0.05$ vs $\text{GaPd}_{12}\text{P}_8$ and $\text{TlPd}_{12}\text{P}_8$.

Antiviral Activity. The antiviral activity of the selected two POPs was investigated against two herpetic viruses, HSV-2 and HCMV, analyzing their ability to reduce the number of viral plaques or foci, respectively, in cell cultures. To this aim, assays were performed by incubating cells in the presence of increasing concentrations of the polyanions before, during, and after viral adsorption. As reported in Figure 6, $\text{GaPd}_{12}\text{P}_8$ and $\text{TlPd}_{12}\text{P}_8$ exhibited an antiviral activity against the two viruses generating dose–response curves. In detail, $\text{GaPd}_{12}\text{P}_8$ exhibited an inhibitory effect with EC_{50} values of 0.21 and 0.44 μM against HSV-2 and HCMV, respectively. Also, $\text{TlPd}_{12}\text{P}_8$ was able to inhibit HSV-2 and HCMV replication with EC_{50} values of 1.02 μM vs 12.56 μM , respectively. Furthermore, the indium(III)-centered analogue $\text{InPd}_{12}\text{P}_8$ ^{8b} was assessed, and a remarkable antiviral activity was demonstrated against both viruses (EC_{50} values of 0.26 μM against HSV-2 and 1.08 μM against HCMV). These data evidenced an antiviral activity against HSV-2 greater than HCMV by all three POPs. Of note, $\text{GaPd}_{12}\text{P}_8$ and $\text{InPd}_{12}\text{P}_8$ exhibited the best antiviral activity against HSV-2 infection amongst the POMs reported in the literature,¹⁶ with an EC_{50} value lower of at least 1 log than the previously reviewed POMs.¹⁷ By contrast, $\text{GaPd}_{12}\text{P}_8$ and $\text{InPd}_{12}\text{P}_8$ exerted an EC_{50} similar or slightly lower than the previously studied POMs against HCMV. In order to ascertain that the antiviral activity was not a consequence of cell toxicity, cell viability assays were performed by incubating the cells with the polyanions under the same conditions used for the antiviral assays in order to determine the half-maximal cytotoxic concentration (CC_{50}) (Figure 7). A difference of two logarithms was evidenced mainly for $\text{GaPd}_{12}\text{P}_8$ and $\text{InPd}_{12}\text{P}_8$ between the CC_{50} values and the EC_{50} values, demonstrating that the polyanions are not toxic at the concentrations used in the antiviral assays (Table 3). In order to identify antiviral candidates, an evaluation of the selectivity index (SI) is fundamental, i.e., the parameter that measures the relative effectiveness of a compound in inhibiting viral replication with respect to its cytotoxicity. In this regard, $\text{GaPd}_{12}\text{P}_8$ exhibited

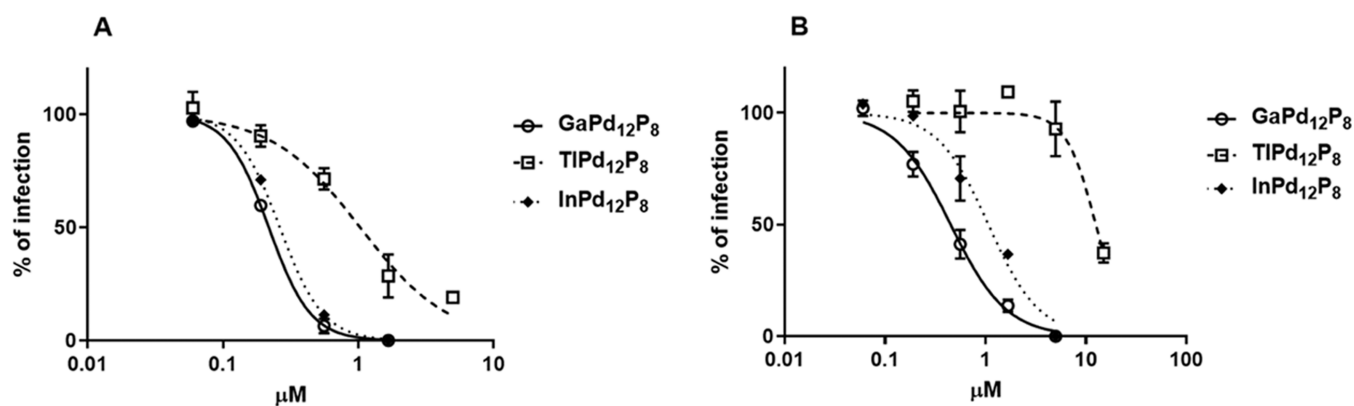


Figure 6. Antiviral activity of GaPd₁₂P₈, TIPd₁₂P₈, and InPd₁₂P₈ against HSV-2 (A) and HCMV (B). On the X-axis, the concentrations of the polyanions are reported. On the Y-axis, the values indicate the percentage of viral infection in comparison to untreated cells. Values are means ± SEM from three independent experiments performed in duplicate.

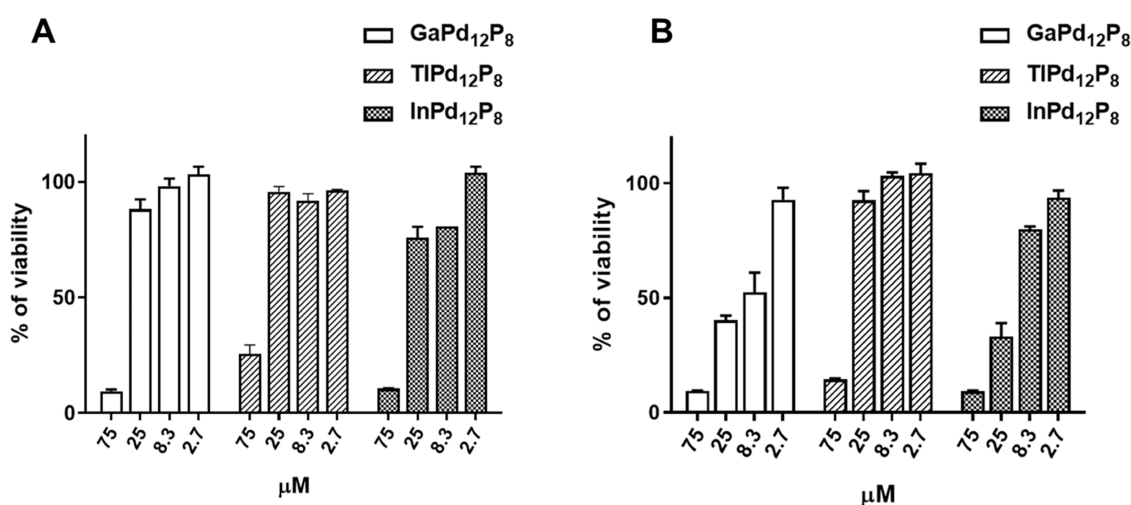


Figure 7. Effect of GaPd₁₂P₈, TIPd₁₂P₈, and InPd₁₂P₈ on the viability of Vero cells (A) as a function of the drug concentrations at 24-h postadministration and on HFF-1 cells (B) at 120-h postadministration. On the X-axis, the concentrations (μM) of the polyanions are reported. On the Y axis, the cell viability is reported as the percentage of viable cells in comparison to the untreated control. The values are reported as means ± SEM for three independent experiments performed in duplicate.

Table 3. Antiviral Activity of GaPd₁₂P₈, TIPd₁₂P₈, and InPd₁₂P₈

compound	virus	EC ₅₀ ^a (μM) (95% CI ^b)	CC ₅₀ ^c (μM) (95% CI)	SI ^d
GaPd ₁₂ P ₈	HCMV	0.44 (0.34–0.57)	13.10 (8.67–19.77)	29.77
	HSV-2	0.21 (0.20–0.23)	41.96 (32.14–54.77)	199.80
TIPd ₁₂ P ₈	HCMV	12.56 (9.78–16.13)	47.75 (37.89–60.18)	3.80
	HSV-2	1.02 (0.79–1.31)	56.46 (46.43–68.66)	55.35
InPd ₁₂ P ₈	HCMV	1.08 (0.71–1.65)	17.37 (15.40–19.59)	16.08
	HSV-2	0.26 (0.24–0.28)	36.41 (26.86–49.35)	140.04

^aEC₅₀: half-maximal effective concentration. ^bCI: confidence interval. ^cCC₅₀: half-maximal cytotoxic concentration. ^dSI: selectivity index (ratio CC₅₀/EC₅₀).

the best SI against both HSV-2 (SI 199.8) and HCMV infection (SI 29.77), making it a favorable candidate for further investigation on its mechanism of antiviral action and drug development.

CONCLUSIONS

In conclusion, the phosphate-capped gallium(III)- and indium(III)-centered polyoxo-12-palladate nanocubes GaPd₁₂P₈ and TIPd₁₂P₈ as well as the phosphate-capped polyoxo-23-palladate double-cube Ti₂Pd₂₃P₁₄ were synthesized and structurally characterized. GaPd₁₂P₈ and TIPd₁₂P₈ were

shown to be solution stable as verified by ³¹P, ⁷¹Ga, and ²⁰⁵Tl NMR. Biological studies demonstrated that GaPd₁₂P₈ and TIPd₁₂P₈ possess antitumor potential and are as efficient as *cis*-platinum against human melanoma and acute promyelocytic leukemia cells. Furthermore, both cuboid POPs exerted inhibitory activity against two enveloped DNA viruses, i.e., HSV-2 and HCMV. The synthesis and structural characterization of three novel gallium- and thallium-centered POPs further expands the class of discrete, anionic palladium-oxo clusters, but perhaps most importantly, the promising antimelanoma, antileukemic, and antiviral activities of the

cuboid derivatives $\text{GaPd}_{12}\text{P}_8$ and $\text{TlPd}_{12}\text{P}_8$ should be further investigated for possible real-world applications.

■ ASSOCIATED CONTENT

SI Supporting Information

The Supporting Information is available free of charge at <https://pubs.acs.org/doi/10.1021/acs.inorgchem.3c01530>.

Sodium-oxo-aqua cluster structure, ^{31}P NMR T_1 values, FT-IR spectra, thermograms, ^{31}P NMR spectra, and simulated AX_7 and $\text{AX}_4\text{Y}_2\text{Z}$ spectra (PDF)

Accession Codes

CCDC 2248051–2248052 and 2248265 contain the supplementary crystallographic data for this paper. These data can be obtained free of charge via www.ccdc.cam.ac.uk/data_request/cif, or by emailing data_request@ccdc.cam.ac.uk, or by contacting The Cambridge Crystallographic Data Centre, 12 Union Road, Cambridge CB2 1EZ, UK; fax: +44 1223 336033.

■ AUTHOR INFORMATION

Corresponding Authors

Zhengguo Lin – School of Science, Constructor University, 28759 Bremen, Germany; College of Chemistry and Materials Science, Hebei Normal University, Shijiazhuang 050024, P. R. China; orcid.org/0000-0002-9628-6888; Email: linzhengguo11@163.com

Imre Tóth – Department of Physical Chemistry, University of Debrecen, 4032 Debrecen, Hungary; Email: imre.toth@science.unideb.hu

Ulrich Kortz – School of Science, Constructor University, 28759 Bremen, Germany; orcid.org/0000-0002-5472-3058; Phone: +49 421 200 3235; Email: u.kortz@jacobs-university.de; Fax: +49 421 200 3102

Authors

Tian Ma – School of Science, Constructor University, 28759 Bremen, Germany; orcid.org/0000-0003-2062-4884

Xiang Ma – School of Science, Constructor University, 28759 Bremen, Germany; orcid.org/0000-0003-0683-5378

Jiayao Zhang – School of Science, Constructor University, 28759 Bremen, Germany; orcid.org/0000-0003-2131-4298

Peng Yang – School of Science, Constructor University, 28759 Bremen, Germany; College of Chemistry and Chemical Engineering, Advanced Catalytic Engineering Research Center of the Ministry of Education, Hunan University, Changsha 410082, P. R. China; orcid.org/0000-0002-1404-2047

Tibor Csupász – Department of Physical Chemistry, University of Debrecen, 4032 Debrecen, Hungary

Sonja Misirlic-Dencic – Institute of Medical and Clinical Biochemistry, Faculty of Medicine, University of Belgrade, 11000 Belgrade, Serbia; Center of Excellence for Redox Medicine, 11000 Belgrade, Serbia; orcid.org/0000-0002-8635-4701

Andjelka M. Isakovic – Institute of Medical and Clinical Biochemistry, Faculty of Medicine, University of Belgrade, 11000 Belgrade, Serbia; Center of Excellence for Redox Medicine, 11000 Belgrade, Serbia; orcid.org/0000-0001-5270-709X

David Lembo – Department of Clinical and Biological Sciences, Laboratory of Molecular Virology and Antiviral Research, University of Turin, 10043 Orbassano, Italy; orcid.org/0000-0002-0969-100X

Manuela Donalisio – Department of Clinical and Biological Sciences, Laboratory of Molecular Virology and Antiviral Research, University of Turin, 10043 Orbassano, Italy; orcid.org/0000-0001-7883-1523

Complete contact information is available at:

<https://pubs.acs.org/doi/10.1021/acs.inorgchem.3c01530>

Notes

The authors declare no competing financial interest.

■ ACKNOWLEDGMENTS

U.K. is thankful to the German Science Foundation (DFG-KO-2288/20-1 and DFG-KO-2288/16-1) and Jacobs University for research support. T.M. acknowledges National Natural Science Foundation of China (No. 52203177). Z.L. acknowledges the financial support program from Hebei Province (Grant Nos. B2022205028 and C20220322) and Hebei Normal University (Grant No. L2022B34). P.Y. acknowledges the Natural Science Foundation of China (No. 22001066), the Natural Science Foundation of Hunan Province (2021JJ40049 and 2022JJ20007), the Science and Technology Innovation Program of Hunan Province 2022RC1115, and the Scientific Research Foundation of the Education Department of Hunan Province (21B0028). I.T. and T.C. are thankful for the financial support granted by the Hungarian National Research Development and Innovation Office (NKFIH K-128201). S.M.-D. and A.M.I. received financial support from the Ministry of Education, Science and Technological Development, Republic of Serbia (Grant Agreement No. 451-03-9/2021-14/200110). This research was supported by EU funding within the MUR PNRR Extended Partnership initiative on Emerging Infectious Diseases (Project no. PE00000007, INF-ACT) to D.L. The POP structures in Figures 1–3 and 5 were generated with Diamond, version 3.2 (copyright Crystal Impact GbR).

■ REFERENCES

- (1) (a) Pope, M. T.; Sadakane, M.; Kortz, U. Celebrating Polyoxometalate Chemistry. *Eur. J. Inorg. Chem.* **2019**, 2019, 340–342. (b) Pope, M. T.; Kortz, U. Polyoxometalates. In *Encyclopedia of Inorganic and Bioinorganic Chemistry*; Wiley, 2012. (c) Long, D. L.; Tsunashima, R.; Cronin, L. Polyoxometalates: building blocks for functional nanoscale systems. *Angew. Chem., Int. Ed.* **2010**, 49, 1736–1758. (d) Proust, A.; Thouvenot, R.; Gouzerh, P. Functionalization of polyoxometalates: towards advanced applications in catalysis and materials science. *Chem. Commun.* **2008**, 1837–1852. (e) Pope, M. T.; Müller, A. Polyoxometalate Chemistry: An Old Field with New Dimensions in Several Disciplines. *Angew. Chem., Int. Ed.* **1991**, 30, 34–48. (f) Pope, M. T. *Heteropoly and Isopoly Oxometalates*; Springer: Berlin, Germany, 1983.
- (2) (a) Čolović, M. B.; Lacković, M.; Lalatović, J.; Mougharbel, A. S.; Kortz, U.; Krstić, D. Z. Polyoxometalates in Biomedicine: Update and Overview. *Curr. Med. Chem.* **2020**, 27, 362–379. (b) Bijelic, A.; Aureliano, M.; Rompel, A. Polyoxometalates as Potential Next-Generation Metallo-drugs in the Combat Against Cancer. *Angew. Chem., Int. Ed.* **2019**, 58, 2980–2999. (c) Bijelic, A.; Aureliano, M.; Rompel, A. The antibacterial activity of polyoxometalates: structures, antibiotic effects and future perspectives. *Chem. Commun.* **2018**, 54, 1153–1169.
- (3) Yang, P.; Kortz, U. Discovery and Evolution of Polyoxopalladates. *Acc. Chem. Res.* **2018**, 51, 1599–1608.
- (4) (a) Barsukova-Stuckart, M.; Izarova, N. V.; Jameson, G. B.; Ramachandran, V.; Wang, Z.; van Tol, J.; Dalal, N. S.; Ngo Biboum, R.; Keita, B.; Nadjro, L.; Kortz, U. Synthesis and characterization of the dicopper(II)-containing 22-palladate(II)

- [Cu₂^{II}Pd₂^{II}P₁₂^VO₆₀(OH)₈]²⁰⁻. *Angew. Chem., Int. Ed.* **2011**, *50*, 2639–2642. (b) Ayass, W. W.; Miñambres, J. F.; Yang, P.; Ma, T.; Lin, Z.; Meyer, R.; Jaensch, H.; Bons, A.-J.; Kortz, U. Discrete Polyoxopalladates as Molecular Precursors for Supported Palladium Metal Nanoparticles as Hydrogenation Catalysts. *Inorg. Chem.* **2019**, *58*, 5576–5582. (c) Bock, N.; De Clercq, A.; Seidl, L.; Kratky, T.; Ma, T.; Günther, S.; Kortz, U.; Heiz, U.; Esch, F. Towards Size-Controlled Deposition of Palladium Nanoparticles from Polyoxometalate Precursors: An Electrochemical Scanning Tunneling Microscopy Study. *ChemElectroChem* **2021**, *8*, 1280–1288. (d) Isakovic, A. M.; Čolović, M. B.; Ma, T.; Ma, X.; Jeremic, M.; Gerić, M.; Gajski, G.; Misirlic-Dencic, S.; Kortz, U.; Krstic, D. Selected polyoxopalladates as promising and selective antitumor drug candidates. *J. Biol. Inorg. Chem.* **2021**, *26*, 957–971. (e) Yang, P.; Mahmoud, M. E.; Xiang, Y.; Lin, Z.; Ma, X.; Christian, J. H.; Bindra, J. K.; Kinyon, J. S.; Zhao, Y.; Chen, C.; Nisar, T.; Wagner, V.; Dalal, N. S.; Kortz, U. Host–Guest Chemistry in Discrete Polyoxo-12-Palladate(II) Cubes [MO₈Pd₁₂L₈]ⁿ⁻ (M = Sc^{III}, Co^{II}, Cu^{II}, L = AsO₄³⁻; M = Cd^{II}, Hg^{II}; L = PhAsO₃²⁻): Structure, Magnetism, and Catalytic Hydrogenation. *Inorg. Chem.* **2022**, *61*, 18524–18535.
- (5) Chubarova, E. V.; Dickman, M. H.; Keita, B.; Nadjo, L.; Miserque, F.; Mifsud, M.; Arends, I. W.; Kortz, U. Self-assembly of a heteropolyoxopalladate nanocube: [Pd₁₃^{II}As₈^VO₃₄(OH)₆]⁸⁻. *Angew. Chem., Int. Ed.* **2008**, *47*, 9542–9546.
- (6) (a) Izarova, N. V.; Biboum, R. N. N.; Keita, B.; Mifsud, M.; Arends, I. W. C. E.; Jameson, G. B.; Kortz, U. Self-assembly of star-shaped heteropoly-15-palladate(II). *Dalton Trans.* **2009**, 9385–9387. (b) Delferro, M.; Graiff, C.; Elviri, L.; Predieri, G. Self-assembly of polyoxoselenopalladate nanostars [Pd₁₅(μ₃-SeO₃)₁₀(μ₃-O)₁₀Na]⁹⁻ and their supramolecular pairing in the solid state. *Dalton Trans.* **2010**, 39, 4479–4481. (c) Yang, P.; Xiang, Y.; Lin, Z.; Bassil, B. S.; Cao, J.; Fan, L.; Fan, Y.; Li, M.-X.; Jimenez-Lozano, P.; Carbo, J. J.; Poblet, J. M.; Kortz, U. Alkaline Earth Guests in Polyoxopalladate Chemistry: From Nanocube to Nanostar via an Open-Shell Structure. *Angew. Chem., Int. Ed.* **2014**, *53*, 11974–11978. (d) Scullion, R. A.; Surman, A. J.; Xu, F.; Mathieson, J. S.; Long, D.-L.; Haso, F.; Liu, T.; Cronin, L. Exploring the symmetry, structure, and self-assembly mechanism of a gigantic seven-fold symmetric {Pd₈₄} wheel. *Angew. Chem., Int. Ed.* **2014**, *53*, 10032–10037.
- (7) (a) Bhattacharya, S. Discrete, Cationic Palladium(II)-Oxo Clusters via f-Metal Ion Incorporation and their Macrocyclic Host-Guest Interactions with Sulfonatocalixarenes. *Angew. Chem., Int. Ed.* **2022**, *61*, e202203114. (b) Bhattacharya, S.; Ma, X.; Mougharbel, A. S.; Haouas, M.; Su, P.; Espenship, M. F.; Taffa, D. H.; Jaensch, H.; Bons, A.-J.; Stuerzer, T.; Wark, M.; Laskin, J.; Cadot, E.; Kortz, U. Discovery of a Neutral 40-Pd^{II}-Oxo Molecular Disk, [Pd₄₀O₂₄(OH)₁₆{(CH₃)₂AsO₂}]₁₆: Synthesis, Structural Characterization and Catalytic Studies. *Inorg. Chem.* **2021**, *60*, 17339–17347. (c) Bhattacharya, S.; Basu, U.; Haouas, M.; Su, P.; Espenship, M. F.; Wang, F.; Solé-Daura, A.; Taffa, D. H.; Wark, M.; Poblet, J. M.; Laskin, J.; Cadot, E.; Kortz, U. Discovery and Supramolecular Interactions of Neutral Palladium-Oxo Clusters Pd₁₆ and Pd₂₄. *Angew. Chem., Int. Ed.* **2021**, *60*, 3632–3639.
- (8) (a) Lang, Z.; Yang, P.; Lin, Z.; Yan, L.; Li, M. X.; Carbó, J. J.; Kortz, U.; Poblet, J. M. Size and charge effect of guest cations in the formation of polyoxopalladates: a theoretical and experimental study. *Chem. Sci.* **2017**, *8*, 7862–7872. (b) Ma, T.; Yang, P.; Parris, J.; Csupas, T.; Li, M. X.; Bányai, I.; Tóth, I.; Lin, Z.; Kortz, U. Indium in Polyoxopalladate(II) Chemistry: Synthesis of All-Acetate-Capped [InPd₁₂O₈(OAc)₁₆]⁵⁻ and Controlled Transformation to Phosphate-Capped Double-Cube and Monocube. *Inorg. Chem.* **2019**, *58*, 15864–15871. (c) Lin, Z.; Wang, B.; Cao, J.; Chen, B.; Xu, C.; Huang, X.; Fan, Y.; Hu, C. Controlled Synthesis of Polyoxopalladates, and Their Gas Phase Fragmentation Study by Electrospray Ionization Tandem Mass Spectrometry. *Eur. J. Inorg. Chem.* **2013**, *2013*, 3458–3463.
- (9) Yang, P.; Ma, T.; Lang, Z. L.; Misirlic-Dencic, S.; Isakovic, A. M.; Bényei, A.; Čolović, M. B.; Markovic, I.; Krstić, D. Z.; Poblet, J. M.; Lin, Z.; Kortz, U. Tetravalent Metal Ion Guests in Polyoxopalladate Chemistry: Synthesis and Anticancer Activity of [MO₈Pd₁₂(PO₄)₈]¹²⁻ (M = Sn^{IV}, Pb^{IV}). *Inorg. Chem.* **2019**, *58*, 11294–11299.
- (10) (a) Ayass, W. W.; Fodor, T.; Lin, Z.; Smith, R. M.; Xing, X.; Abdallah, K.; Tóth, I.; Zékány, L.; Pascual-Borràs, M.; Rodríguez-Fortea, A.; Poblet, J. M.; Fan, L.; Cao, J.; Keita, B.; Ullrich, M. S.; Kortz, U. Synthesis, Structure, and Antibacterial Activity of a Thallium(III)-Containing Polyoxometalate, [Tl₂{B-β-Si-W₈O₃₀(OH)}₂]¹²⁻. *Inorg. Chem.* **2016**, *55*, 10118–10121. (b) Ayass, W. W.; Fodor, T.; Farkas, E.; Lin, Z.; Qasim, H. M.; Bhattacharya, S.; Mougharbel, A. S.; Abdallah, K.; Ullrich, M. S.; Zaib, S.; Iqbal, J.; Harangi, S.; Szalontai, G.; Bányai, I.; Zékány, L.; Tóth, I.; Kortz, U. Dithallium(III)-Containing 30-Tungsto-4-phosphate, [Tl₂Na₂(H₂O)₂(P₂W₁₅O₅₆)₂]¹⁶⁻: Synthesis, Structural Characterization, and Biological Studies. *Inorg. Chem.* **2018**, *57*, 7168–7179.
- (11) (a) Misirlic-Dencic, S.; Poljarevic, J.; Isakovic, A. M.; Markovic, I.; Sabo, T. J.; Grgurić-Šipka, S. Antileukemic action of novel diamine Pt(II) halogenido complexes: Comparison of the representative novel Pt(II) with corresponding Pt(IV) complex. *Chem. Biol. Drug. Des.* **2017**, *90*, 262–271. (b) Misirlic-Dencic, S.; Poljarevic, J.; Vilimanovic, U.; Bogdanovic, A.; Isakovic, A. J.; Stevovic, T. K.; Dulovic, M.; Zogovic, N.; Isakovic, A. M.; Grguric-Sipka, S.; Bumbasirevic, V.; Sabo, T.; Trajkovic, V.; Markovic, I. Cyclohexyl Analogues of Ethylenediamine Dipropionic Acid Induce Caspase-Independent Mitochondrial Apoptosis in Human Leukemic Cells. *Chem. Res. Toxicol.* **2012**, *25*, 931–939.
- (12) Toujani, M. M.; Rittà, M.; Civra, A.; Genovese, S.; Epifano, F.; Ghram, A.; Lembo, D.; Donalizio, M. Inhibition of HSV-2 infection by pure compounds from Thymus capitatus extract in vitro. *Phytother. Res.* **2018**, *32*, 1555–1563.
- (13) Donalizio, M.; Cagno, V.; Vallino, M.; Moro, G. E.; Arslanoglu, S.; Tonetto, P.; Bertino, E.; Lembo, D. Inactivation of high-risk human papillomaviruses by Holder pasteurization: implications for donor human milk banking. *J. Perinat. Med.* **2014**, *42*, 1–8.
- (14) Donalizio, M.; Argenziano, M.; Rittà, M.; Bastiancich, C.; Civra, A.; Lembo, D.; Cavalli, R. Acyclovir-loaded sulfobutyl ether-beta-cyclodextrin decorated chitosan nanodroplets for the local treatment of HSV-2 infections. *Int. J. Pharm.* **2020**, *587*, No. 119676.
- (15) Yang, P. Synthesis, Characterization and Properties of Polyoxopalladates and Organoantimony(III)-Substituted Heteropolytungstates, Ph.D. Thesis; Jacobs University, 2016.
- (16) Dan, K.; Miyashita, K.; Seto, Y.; Fujita, H.; Yamase, T. Mechanism of the protective effect of heteropolyoxotungstate against herpes simplex virus type 2. *Pharmacology* **2003**, *67*, 83–89.
- (17) (a) Inouye, Y.; Tokutake, Y.; Yoshida, T.; Seto, Y.; Hujita, H.; Dan, K.; Yamamoto, A.; Nishiya, S.; Yamase, T.; Nakamura, S. In vitro antiviral activity of polyoxomolybdates. Mechanism of inhibitory effect of PM-104 (NH₄)₁₂H₂(Eu₄(MoO₄(H₂O))₁₆(Mo₇O₂₄)₄)·13H₂O on human immunodeficiency virus type 1. *Antiviral Res.* **1993**, *20*, 317–331. (b) Rhule, J. T.; Hill, C. L.; Judd, D. A.; Schinazi, R. F. Polyoxometalates in medicine. *Chem. Rev.* **1998**, *98*, 327–357. (c) Wang, J.; Liu, Y.; Xu, K.; Qi, Y. F.; Zhong, J.; Zhang, K.; Li, J.; Wang, E. B.; Wu, Z. Y.; Kang, Z. H. Broad-Spectrum Antiviral Property of Polyoxometalate Localized on a Cell Surface. *ACS Appl. Mater. Interfaces* **2014**, *6*, 9785–9789. (d) Yamamoto, N.; Schols, D.; De Clercq, E.; Debyser, Z.; Pauwels, R.; Balzarini, J.; Nakashima, H.; Baba, M.; Hosoya, M.; Snoeck, R.; Neyts, J.; Andrei, G.; Murrer, B. A.; Theobald, B.; Bossard, G.; Henson, G.; Abrams, M.; Picker, D. Mechanism of anti-human immunodeficiency virus action of polyoxometalates, a class of broad-spectrum antiviral agents. *Mol. Pharmacol.* **1992**, *42*, 1109–1117. (e) Ikeda, S.; Neyts, J.; Yamamoto, N.; Murrer, B.; Theobald, B.; Bossard, G.; Henson, G.; Abrams, M.; Picker, D.; De Clercq, E. In vitro activity of a novel series of polyoxosilicotungstates against human myxo-, herpes-, and retroviruses. *Antiviral Chem. Chemother.* **1993**, *4*, 253–262.